Advances in Atmospheric Sciences
Impact Factor: 3.158
E-alert
ISSN 0256-1530
CN 11-1925/O4

Impact of the Western Pacific Tropical Easterly Jet on Tropical Cyclone Genesis Frequency over the Western North Pacific

Ruifen ZHAN, Yuqing WANG, Yihui DING

Citation: Zhan, R. F., Y. Q. Wang, Y. H. Ding, 2022: Impact of the Western Pacific Tropical Easterly Jet on Tropical Cyclone Genesis Frequency over the Western North Pacific, *Adv. Atmos. Sci.*, In press. doi: 10.1007/s00376-021-1103-1.

View online: https://doi.org/10.1007/s00376-021-1103-1

ADVANCES IN ATMOSPHERIC SCIENCES, VOL. 39, FEBRUARY 2022, 235–248

• **Original Paper** •

Impact of the Western Pacific Tropical Easterly Jet on Tropical Cyclone Genesis Frequency over the Western North Pacific※

Ruifen ZHAN*[1,2,3], Yuqing WANG[4], and Yihui DING[5]

[1]*Department of Atmospheric and Ocean Sciences*, *Institute of Atmospheric Sciences*, *Fudan University*, *Shanghai* 200438, *China*

[2]*Shanghai Typhoon Institute of China Meteorological Administration*, *Shanghai* 200030, *China*

[3]*Innovation Center of Ocean and Atmosphere System*, *Zhuhai Fudan Innovation Research Institute*, *Zhuhai* 519055, *China*

[4]*International Pacific Research Center and Department of Atmospheric Sciences*, *School of Ocean and Earth Science and Technology*, *University of Hawaii at Manoa*, *Honolulu*, *Hawaii*, *HI* 96822, *USA*

[5]*National Climate Center and Laboratory for Climate Studies*, *China Meteorological Administration*, *Beijing* 100081, *China*

(Received 9 March 2021; revised 10 July 2021; accepted 12 August 2021)

ABSTRACT

Although it is well known that the tropical easterly jet (TEJ) has a significant impact on summer weather and climate over India and Africa, whether the TEJ exerts an important impact on tropical cyclone (TC) activity over the western North Pacific (WNP) remains unknown. In this study, we examined the impact of the TEJ on the interannual variability of TC genesis frequency over the WNP in the TC season (June–September) during 1980–2020. The results show a significant positive correlation between TC genesis frequency over the WNP and the jet intensity in the entrance region of the TEJ over the tropical western Pacific (in brief WP_TEJ), with a correlation coefficient as high as 0.66. The intensified WP_TEJ results in strong ageostrophic northerly winds in the entrance region and thus upper-level divergence to the north of the jet axis over the main TC genesis region in the WNP. This would lead to an increase in upward motion in the troposphere with enhanced low-level convergence, which are the most important factors to the increases in low-level vorticity, mid-level humidity and low-level eddy kinetic energy, and the decreases in sea level pressure and vertical wind shear in the region. All these changes are favorable for TC genesis over the WNP and vice versa. Further analyses indicate that the interannual variability of the WP_TEJ intensity is likely to be linked to the local diabatic heating over the Indian Ocean-western Pacific and the central Pacific El Niño-Southern Oscillation.

Key words: tropical cyclones, genesis frequency, tropical easterly jet, western North Pacific

Citation: Zhan, R. F., Y. Q. Wang, and Y. H. Ding, 2022: Impact of the western Pacific tropical easterly jet on tropical cyclone genesis frequency over the western North Pacific. *Adv. Atmos. Sci.*, **39**(2), 235–248, https://doi.org/10.1007/s00376-021-1103-1.

Article Highlights:

- A strong link exists between the WP_TEJ intensity and WNP TC genesis frequency on the interannual timescale.
- The intensified WP_TEJ results in ageostrophic northerly winds in the entrance region with upper-level divergence to the north, favorable for WNP TC genesis.
- The WP_TEJ intensity might be related to the western Pacific summer monsoon rainfall and ENSO Modoki.

1. Introduction

Tropical cyclone (TC) genesis is one of the most important aspects of TC activity. What determines the variability of TC genesis frequency (TCGF) is a scientific concern that has attracted great attention over the past 2–3 decades. However, our current understanding of the controlling factors and the predominant processes are far from complete (Emanuel, 2018). Understanding the processes driving TCGF over the western North Pacific (WNP) is particularly difficult because in this basin the large-scale ocean and

※ This paper is a contribution to the special issue on Climate Change and Variability of Tropical Cyclone Activity.

* Corresponding author: Ruifen ZHAN
Email: zhanrf@fudan.edu.cn

atmospheric circulations are subject to variabilities on various timescales and involving strong nonlinear interactions. Among the various timescales, the variability of TCGF over the WNP on the interannual timescale is pronounced and the most important for seasonal prediction of TC activity (Chan, 2005; Zhan et al., 2012). For example, the WNP witnessed 34 named TCs in 1994 but only 14 in 2010. Thus, improving our understanding about the large-scale climate factors and the controlling processes on the interannual variability of TCGF over the WNP is of scientific and social importance.

Many previous studies have emphasized the importance of oceanic factors in affecting the interannual variability of TCGF over the WNP (see a review by Klotzbach et al., 2019). It has been well recognized that the El Niño–Southern Oscillation (ENSO), the strongest interannual climate signal on Earth, plays an important role in controlling TC genesis location and frequency depending on the warming patterns (Chia and Ropelewski, 2002; Wang and Chan, 2002; Chen and Tam, 2010). There is a significant eastward displacement of the mean location of TC genesis over the WNP in the El Niño years when the warming occurs in the equatorial eastern Pacific, while there is a significant increase in TCGF over the WNP in the El Niño years when the warming occurs in the equatorial central Pacific. These differences have been found to be linked to the different responses of atmospheric circulations over the WNP to the warming–induced convective activity at different locations (Chen and Tam, 2010; Wu et al., 2018). Other oceanic factors, such as sea surface temperature (SST) anomalies in the East Indian Ocean and Atlantic Ocean, the spring SST gradient between the southwest Pacific and the western Pacific warm pool (SSTG), and the Pacific meridional mode, also exert profound influences on the interannual variability of TCGF over the WNP (Zhan et al., 2011, 2013; Yu et al., 2016; Zhang et al., 2016). Recently, Zhan et al. (2019) quantitatively evaluated contributions of several key SST factors in the Indo-Pacific Oceans to the interannual variability of WNP TCGF and found that the spring SSTG and East Indian Ocean SST anomalies contribute the most (about 77%).

In addition to the oceanic factors, large-scale atmospheric circulations also exert important controls on the interannual variability of TCGF over the WNP (Chan, 2005; Wang et al., 2007; Zhou and Cui, 2008; Guo and Tan, 2018). In particular, some studies have demonstrated that upper tropospheric environmental forcing can affect TC genesis and development (e.g., Pfeffer and Challa, 1981; Sears and Velden, 2014; Wang and Wu, 2016; Fischer et al., 2017, 2019; Wang and Wang, 2021). This is because favorable upper-tropospheric forcing can enhance ascending motion in the region of TC genesis or near the TC center or accelerate the outflow channels. Such outflow channels in the upper troposphere could provide favorable conditions for TC genesis and development against the comparatively weak environmental resistance (Sears and Velden, 2014).

The tropical easterly jet (TEJ), which was first discovered by Koteswaram (1958), is among the most conspicuous upper-level environmental features in boreal summer (usually June–September). The TEJ has two centers observed at 150–200 hPa (Krishnamurti and Bhalme, 1976; Fontaine and Janicot, 1992; Huang et al., 2020). The stronger one originates from the differential heating between the Tibetan Plateau and the Indian Ocean and extends eastward into the tropical western Pacific, and the weaker one is located over the tropical eastern Pacific. The inflow region of the TEJ over the tropical western Pacific is split into two branches with the northern branch near 20°N and the southern branch near 5°N (Lu and Ding, 1989; Liang, 1990). The southern branch TEJ (hereafter WP_TEJ) is generally stronger than the northern branch and extends further eastward-southeastward (Fig. 1). Previous studies have indicated that the TEJ exerts great impacts on tropical weather and climate (Krishnamurti and Bhalme, 1976; Besson and Lemaître, 2014; Li et al., 2017; Vashisht et al., 2021). It is well documented that upper-level divergence south of the TEJ exit region or north of the TEJ entrance region can promote convection by forcing ascent and low-level convergence in accordance with Dines compensation. The opposite is true for the upper-level convergence north of the exit region and south of the entrance region of the TEJ (e.g., Uccellini and Johnson, 1979).

Several studies have also revealed the relationship between the TEJ and TC activity on the interannual and decadal variabilities (Chen, 2006; Rao et al., 2008; Krishnamurti et al., 2018). It has been hypothesized that over the North Indian Ocean the weakened TEJ tends to induce more TCs with above-hurricane intensities by reducing large-scale vertical wind shear (Rao et al., 2008). The TEJ over the coast of West Africa provides favorable conditions for the strongest Atlantic hurricanes in recent years (Krishnamurti et al., 2018). Chen (2006) found a significant negative correlation between the TEJ intensity over the Arabian Sea and TCGF over the WNP. However, how the TEJ over the Arabian Sea affects WNP TCGF remains unknown.

As mentioned above, the TEJ over the tropical western Pacific has two branches, which are in the entrance region of the major TEJ over the southern and southeastern Asia (Fig. 1), implying that these two TEJ branches might be important for weather and climate, such as the activity of TCs over the WNP as well. However, little attention has been given to the role of these two branches in affecting TC activity over the WNP. This is not surprising since the main TEJ core is most often located over the North Indian Ocean (Krishnamurti and Bhalme, 1976; Fontaine and Janicot, 1992; Nicholson, 2009). In fact, it is interesting to note that WNP TCs predominantly form to the north of the entrance region of the WP_TEJ (Fig. 1), indicating a possible linkage between the WP_TEJ and TC genesis over the WNP. Zhang (1986) reported that the WP_TEJ was closely correlated with TC count in August over the WNP with more TCs forming in strong WP_TEJ months based on the observed

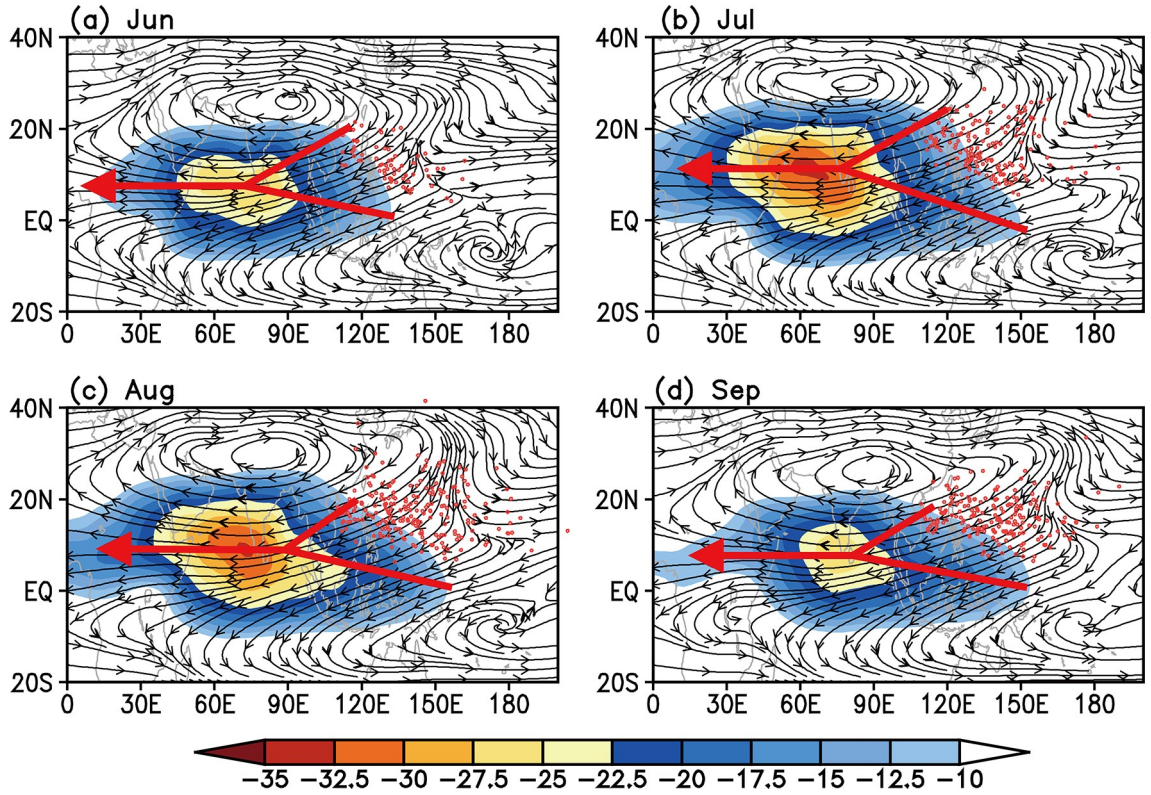

Fig. 1. The climatological mean monthly 150-hPa horizontal wind (vectors, m s^{-1}) and its zonal component (shaded, m s^{-1}) from June to September averaged for the period 1980–2020, and monthly TC genesis locations (red dots) from June to September accumulated from 1980–2020 for: (a) June; (b) July; (c) August; and (d) September. The thick red lines denote the TEJ.

data during 1968–81. However, this earlier study did not provide detailed analysis on how and to what extent the WP_TEJ may affect TCGF over the WNP. Therefore, further work over a longer period of time and using more advanced data analysis is needed to gain a more comprehensive understanding of the interannual relationship between the WP_TEJ and TCGF over the WNP, which would also enrich the understanding of the process driving WNP TC genesis in general.

The main objective of this study is to examine the impact of the WP_TEJ on the interannual variability of TCGF over the WNP in the TC season (June–September) during 1980–2020 and the involved physical mechanisms based on the best track TC data and global reanalysis. We will show that a strong link exists between the WP_TEJ intensity and WNP TCGF on the interannual timescale. The intensified (weakened) WP_TEJ may result in strong (weak) ageostrophic northerly winds in the entrance region of the WP_TEJ, thus enhancing (reducing) divergence in the upper troposphere and upward motion below and low-level convergence to the north of the jet axis in the main TC genesis region, favorable (unfavorable) for TC genesis over the WNP. The rest of the paper is organized as follows. The data and methodology are described in section 2. Climatological characteristics of the WP_TEJ are presented in section 3. The correlation between the WP_TEJ and TCGF over the WNP is analyzed in section 4. Section 5 explores how the WP_TEJ modulates the large-scale environmental conditions and thus affects TCGF over the WNP. Conclusions and discussion are given in the last section.

2. Data and methodology

2.1. *Data*

The TC best-track dataset over the WNP, including the maximum sustained 10-m wind speed and location information with a 6-hour interval for each TC during 1980–2020 was obtained from the Shanghai Typhoon Institute (STI) of the China Meteorological Agency (CMA). The TC best-track datasets from the Japan Meteorological Agency (JMA) and the Joint Typhoon Warning Center (JTWC) were used to confirm the robustness of the results based on the CMA best-track dataset. We focused on TCs with at least tropical storm intensity (with maximum sustained 10-m wind speed $\geqslant$ 17 m s^{-1}) in the TC season each year during 1980–2020. Here, the TC season is defined as the period from June to September because the TEJ prevails during this period.

The monthly and daily National Centers for Environmental Prediction and National Center for Atmospheric Research (NCEP/NCAR) reanalysis data with a horizontal resolution of 2.5° × 2.5° (Kalnay et al., 1996) were utilized to examine large-scale environmental fields. In addition, the

monthly extended reconstructed SST data (ERSST v5) from the National Oceanic and Atmospheric Administration (NOAA; Smith and Reynolds, 2004), and the monthly Climate Prediction Center (CPC) Merged Analysis of Precipitation data (CMAP; Xie and Arkin, 1997) were also used in this study.

2.2. *Methodology*

According to quasi-geostrophic theory, jet streaks are subject to substantial ageostrophic flows in their entrance and exit regions. Following Chen et al. (2007), the equation of motion for the zonal wind component can be used to discuss the ageostrophic motion associated with the TEJ, which can be given as

$$\frac{\mathrm{d}u}{\mathrm{d}t} = f(v - v_{\mathrm{g}}) = f v_{\mathrm{ag}}\,, \tag{1}$$

where u, v are the zonal and meridional wind components, respectively, v_{g} is the meridional component of geostrophic wind, and v_{ag} is the meridional component of ageostrophic flow. Equation (1) predicts two asymmetric divergence–convergence couplets with the upper-level divergence (convergence) along the poleward side of the jet entrance (exit) and the equatorward side of the exit (entrance) region of the TEJ (e.g., Uccellini and Johnson, 1979; Lemburg, 2019). It should be noted that this equation may be not completely applicable for the region near the equator south of the WP_TEJ as the Coriolis force becomes negligible there.

The eddy kinetic energy (EKE) can well represent the activity of mesoscale and synoptic disturbances, which provides favorable conditions for TC genesis. The EKE can be written as

$$\mathrm{EKE} = \frac{1}{2}(\overline{u'^2} + \overline{v'^2})\,, \tag{2}$$

where u' and v' represents the zonal and meridional wind components of the eddy or synoptic motions defined as their deviations from their corresponding basic states, which are defined as an 11-day running mean of their corresponding daily values. The overbar means the time mean during a TC season in each year during the study period.

Since low-level relative vorticity is one of the dominant atmospheric factors controlling TC genesis (Gray, 1968), the relative vorticity tendency equation was adopted to determine the main processes contributing to the low-level vorticity anomalies associated with changes in the WP_TEJ using daily NCEP/NCAR reanalysis data. Ignoring the effects of surface friction and turbulent mixing, the relative vorticity tendency equation in pressure coordinates can be written as (Holton and Staley, 1973):

$$\frac{\partial \zeta}{\partial t} = -\left(u\frac{\partial \zeta}{\partial x} + v\frac{\partial \zeta}{\partial y} + \frac{\partial f}{\partial y}v\right) - \omega\frac{\partial \zeta}{\partial p} - (f+\zeta)\times \left(\frac{\partial u}{\partial x} + \frac{\partial v}{\partial y}\right) + \left(\frac{\partial \omega}{\partial y}\frac{\partial u}{\partial p} - \frac{\partial \omega}{\partial x}\frac{\partial v}{\partial p}\right)\,, \tag{3}$$

where ζ and f represent the relative vorticity and the Coriolis parameter, u, v and ω represent the zonal wind, meridional wind, and vertical p-velocity, respectively. The vorticity tendency is determined by the four terms on the right-hand side of Eq. (3): the horizontal advection of the absolute vorticity (HADV), the vertical advection of the relative vorticity (VADV), the divergence (DIV) term, and the tilting term (TILT), in that order.

The dynamic genesis potential index (DGPI) proposed by Wang and Murakami (2020) was used to examine the importance of large-scale dynamic conditions for TC genesis because it can capture the interannual variability of TCGF over the WNP (Wang and Murakami, 2020; Wang et al., 2021). The DGPI is given as:

$$\mathrm{DGPI} = (2 + 0.1V_{\mathrm{s}})^{-1.7}(5.5 - \frac{\mathrm{d}u}{\mathrm{d}y}10^5)^{2.3}(5 - 20w)^{3.3}\times (5.5 + |10^5\eta|)^{2.4}e^{-11.8} - 1\,, \tag{4}$$

where V_{s} is the magnitude of vertical wind shear (VWS) between 200 and 850 hPa, du/dy is the meridional gradient of zonal wind at 500 hPa, w is the 500-hPa vertical pressure velocity, and η is the 850-hPa absolute vorticity.

In the following discussion, the interannual component of any variable was calculated by removing the signals with timescales over 10 years from the original data using the fast Fourier transform.

3. Climatological characteristics of the WP_TEJ in boreal summer

Figure 1 shows the climatological monthly mean 150-hPa horizontal wind and its zonal component from June to September in the period 1980–2020. There is a strong upper tropospheric anticyclone over the Tibetan Plateau in boreal summer, with upper-level easterly winds covering most of the tropical regions south of the anticyclone. The TEJ with the monthly mean zonal wind speed maximum exceeding 30 m s^{-1} appears in the upper-level easterlies, extending from the tropical western Pacific to the tropical Atlantic with the center over the North Indian Ocean. As the Tibetan anticyclone (which is also often termed South Asian High) intensifies and shifts northwards, the TEJ strengthens and expands from June to August. Afterwards, the Tibetan anticyclone weakens and withdraws southwards; and accordingly, the TEJ also weakens and shrinks compared to August. Another prominent feature is the two branches of the TEJ over the tropical western Pacific in boreal summer with the northern branch over ~20°N and the southern branch over ~5°N, which has been well documented in previous studies (e.g., Lu and Ding, 1989; Liang, 1990) as mentioned in section 1. These two branches are in the entrance region of the TEJ. Generally, the southern branch is much stronger than the northern branch, extending eastwards from 130°E in June to 150°E in July and continuing until September. In this study, this southern branch is referred to the west-

ern Pacific TEJ, or in short, the WP_TEJ in the following discussion.

Since the WP_TEJ is relatively strong in the region of (5°–10°N, 110°–120°E) in August (Fig. 1), we examined the vertical structure of the climatological August mean zonal wind averaged along 5°–10°N and 110°–120°E, respectively, with the results shown in Fig. 2. The center of the WP_TEJ is located at 150 hPa, similar to that of the TEJ. The core of the jet over the tropical western Pacific expands upward with latitude (Fig. 2b). That is, the center of the WP_TEJ with the maximum in the climatological mean zonal wind exceeding 20 m s^{-1} is lower in height than that of the northern branch with the maximum zonal wind between 15 and 20 m s^{-1}. The climatological characteristics of the mean zonal wind in other months of the typhoon season are very similar to those in August (figures not shown).

4. Correlation between the WP_TEJ intensity and TCGF over the WNP

Figure 1 also gives the climatological monthly TC genesis locations over the WNP during 1980–2020. Most TCs clearly formed north of the WP_TEJ core, indicating a possible linkage between the WP_TEJ and TC genesis over the WNP. In order to confirm the linkage on the interannual timescale, we examined the correlation between the upper-level zonal wind and the TCGF over the WNP during

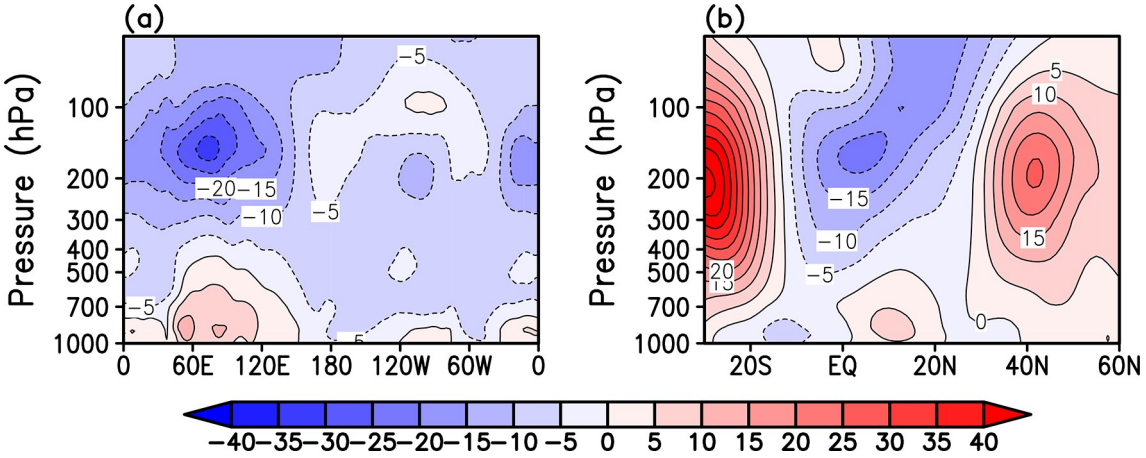

Fig. 2. (a) Longitude-pressure and (b) latitude-pressure sections of the climatological mean zonal wind (m s^{-1}) averaged in August during the period 1980–2020. The plots are averaged for (a) 5°–10°N and (b) 110°–120°E, respectively.

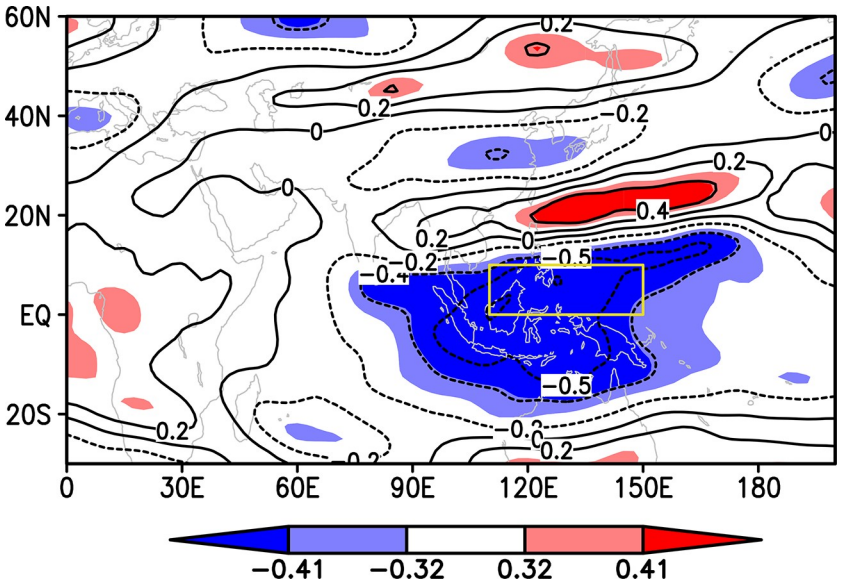

Fig. 3. Correlation coefficients between 150-hPa zonal wind and TCGF over the WNP in the TC season during 1980–2020. The areas with light and dark red (light and dark blue) shades indicate areas where the positive (negative) correlation is statistically significant at the 95% and 99% confidence level based on the Student *t* test, respectively. The yellow box indicates the region used for the definition of the WP_TEJ index.

1980–2020. Figure 3 shows the spatial distributions of the correlation coefficients between the 150-hPa zonal wind and TCGF in the TC season during 1980–2020 based on the CMA best track data. As expected, the WNP TCGF exhibits significant negative correlations with the upper-level zonal wind extending from the tropical East Indian Ocean to the tropical western Pacific with the maximum center over the tropical western Pacific, including the region of the WP_TEJ. Significant positive correlations are mainly located in a narrow belt over the WNP near 20°N. In sharp contrast, the correlation between the TEJ core and WNP TCGF is not statistically significant. According to the above significant negative correlation regions and the climatological location of the WP_TEJ (Fig. 1), we defined the WP_TEJ intensity index as the negative value of 150-hPa zonal wind anomaly averaged over 0°–10°N, 110°–150°E. Note that the negative value of zonal wind anomaly was considered here to make the index consistent with the intensity of the WP_TEJ, which is easterly (negative zonal wind). Namely, the positive (negative) index indicates the strong (weak) WP_TEJ. This definition is not the same as that used in previous studies, e.g., which roughly defined the southern branch TEJ as the 150-hPa zonal wind anomaly at 5°N from the South China Sea to the western Pacific (Yang, 1980) or as that at 5°N, 100°E (Zhang, 1986). Our definition uses a wider region, which can better represent WP_TEJ variability.

Figure 4 shows the normalized time series of the WNP TCGF and the WP_TEJ index averaged over the TC season from 1980 to 2020 based on the original data and the data with the longer-term signal over 10 years removed, respectively. Positive correlation between the WNP TCGF and the WP_TEJ index appears in both the original data and the interannual components, with correlation coefficients of 0.59 and 0.66 (Table 1), respectively, both statistically significant at the 99% confidence level. This suggests that more (fewer) TCs formed in response to the strong (weak) WP_TEJ in the TC season over the WNP. The variation of the WP_TEJ intensity can explain about 44% of the total variance of the interannual variability in WNP TCGF. To confirm this relationship, Table 1 also shows the correlations of the WP_TEJ index and WNP TCGFs using the JTWC and JMA best track datasets. The results are consistent with those using the CMA best track dataset. The correlation coefficients with the WP_TEJ index on the interannual timescale reach 0.53 and 0.51 for the JMA and JTWC best track

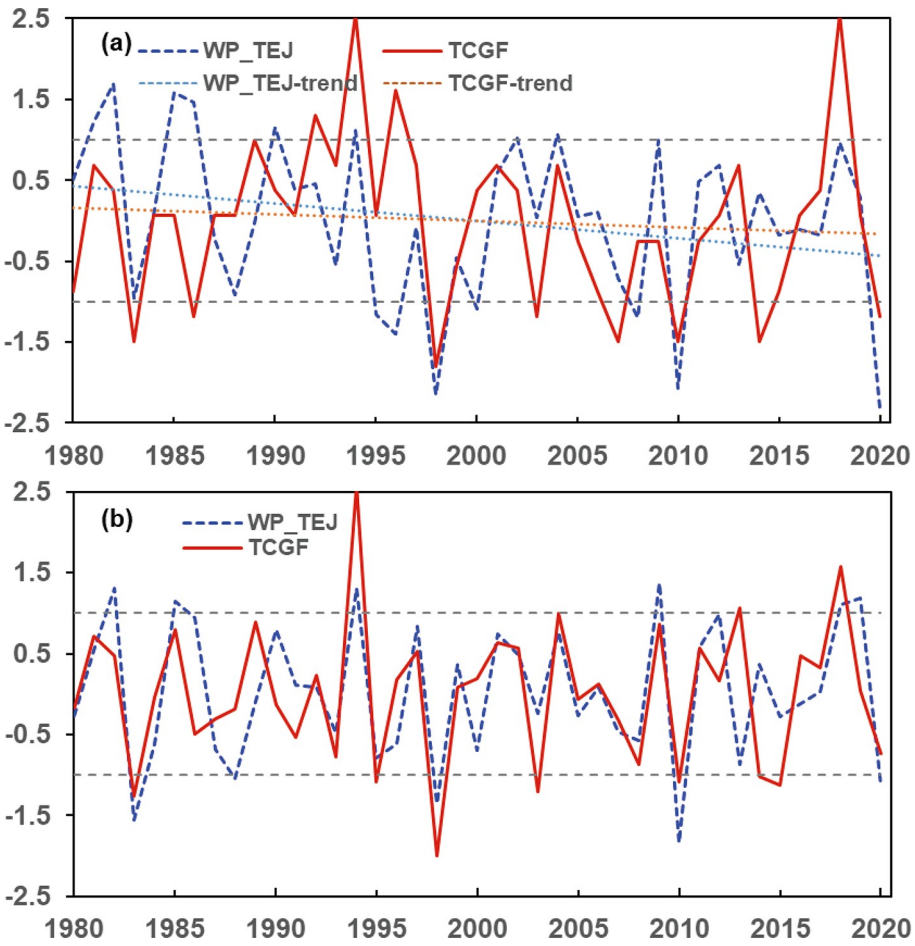

Fig. 4. Normalized time series of the WNP TCGF based on the CMA best track data (orange) and the WP_TEJ index (blue) averaged over the TC season during 1980–2020 using (a) the original data and (b) the interannual components.

Table 1. Correlation coefficients between the WP_TEJ index and the WNP TCGFs averaged in the TC season during 1980–2020 based on original data and interannual components from the CMA, JMA and JTWC best track datasets.

	Correlation coefficients		
	CMA	JMA	JTWC
Original	0.59	0.46	0.38
Interannual	0.66	0.53	0.51

datasets, respectively, which although somewhat lower than that using the CMA dataset, are both statistically significant over the 99% confidence level as well.

To further demonstrate the dependence of WNP TCGF on the WP_TEJ intensity, we defined six strong WP_TEJ years (1982, 1985, 1994, 2009, 2018, and 2019 with the WP_TEJ index ≥ 1 standard deviation) and five weak WP_TEJ years (1983, 1988, 1998, 2010, and 2020 with the WP_TEJ index ≤ -1 standard deviation) based on Fig. 4b on the interannual time scale. It is found that on average there were 19.5 yr^{-1} and 11.6 yr^{-1} in the strong and weak WP_TEJ years, respectively, much more and less than the climatological mean of 15.9 yr^{-1} averaged during 1980–2020. The difference in WNP TCGFs between the strong and weak years is statistically significant at the 95% confidence level based on the Student's *t* test.

5. Possible physical mechanisms

The above statistical analyses suggest that the interannual variability of WNP TCGF is significantly affected by changes in the WP_TEJ intensity. A natural question arises

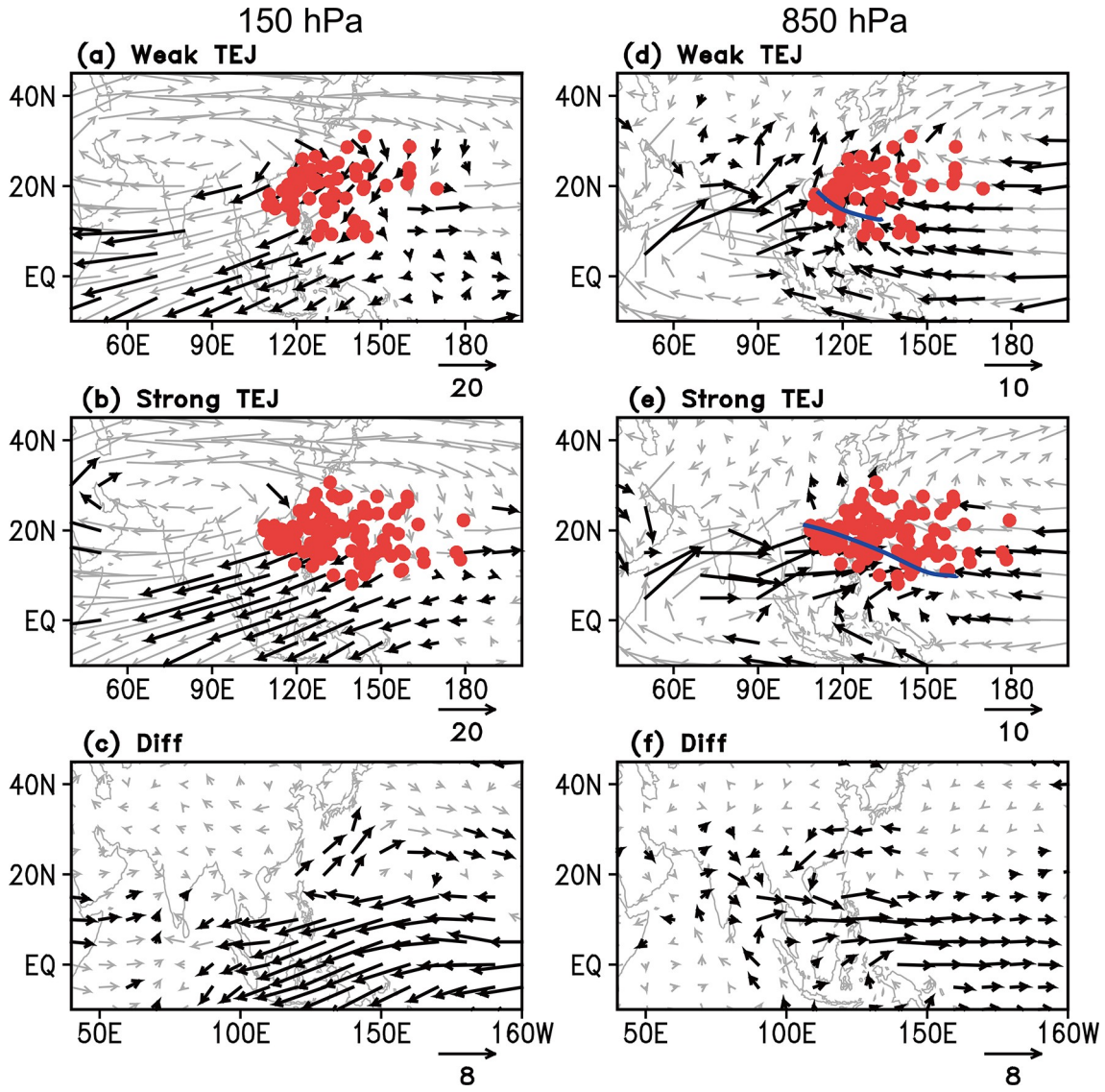

Fig. 5. Composite (left) 150-hPa and (right) 850-hPa wind fields (vector) and TC genesis locations (red dots) for weak WP_TEJ years (a, d) and strong WP_TEJ years (b, e), and the composite differences between the strong and weak WP_TEJ years (c, f). The monsoon trough is denoted by a blue solid line in (d) and (e). Thick arrows indicate areas where the difference is statistically significant at the 95% confidence level by the Student's *t* test.

as to how changes in the WP_TEJ intensity affect TCGF over the WNP. Figure 5 shows the composite 150-hPa and 850-hPa wind fields for strong and weak WP_TEJ years, and their composite differences. The most prominent feature in the wind fields is the enhanced upper-level easterly winds and the deepened low-level monsoon trough over the tropical western Pacific in the strong WP_TEJ years. Correspondingly, the TC genesis locations extended eastward in the strong WP_TEJ years relative to those in the weak WP_TEJ years. As a result, an anomalous upper-level anticyclone and an anomalous low-level cyclone over the WNP can be seen in the composite difference fields, a situation more favorable for TC genesis. In contrast, there is no significant difference in the Tibetan anticyclone between the strong and weak WP_TEJ years, suggesting that the effect of the WP_TEJ on WNP TCGF is independent of the TEJ core over the North Indian Ocean.

We further examined several other large-scale environmental fields that could affect TC genesis over the WNP. Figure 6 shows the regressed 850-hPa vorticity, sea level pressure (SLP), vertical wind shear (VWS), middle tropospheric vertical p-velocity, 600-hPa specific humidity, and 850-hPa EKE with respect to the WP_TEJ index. In response to the strong WP_TEJ, the lower troposphere over the main TC genesis region over the WNP is dominated by cyclonic vorticity anomalies (Fig. 6a), negative SLP anomalies (Fig. 6b) and positive EKE (Fig. 6f). The middle troposphere over the main TC genesis region is covered by anomalous ascending motion (Fig. 6d) and increased specific humidity (Fig. 6e). Meanwhile, the VWS is reduced in the regions north of 20°N and west of 140°E, and south of 20°N and east of 140°E (Fig. 6c). These thermodynamic and dynamic conditions are favorable for TC genesis over the WNP (e.g., Gray, 1968; Zhan et al., 2012; Klotzbach et al., 2019).

To reveal the combined effects and the relative importance of the large-scale dynamical conditions on TC genesis, the DGPI proposed by Wang and Murakami (2020) was analyzed. Figure 7a shows the composite differences in TCGF density and DGPI anomalies over the WNP between the strong and weak WP_TEJ years. As expected, the positive

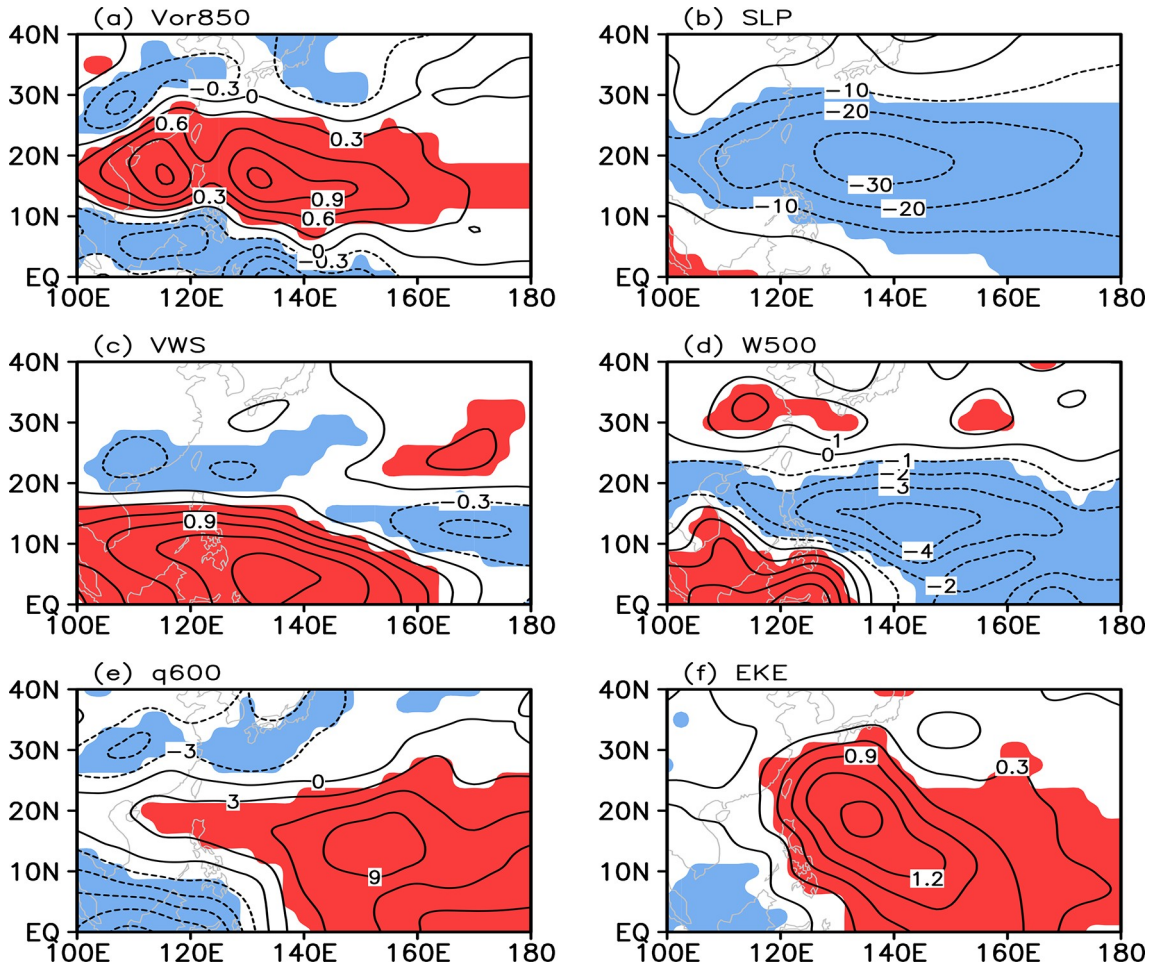

Fig. 6. Regressed patterns of (a) 850-hPa vorticity (Vor850; 10^{-5} s^{-1}), (b) sea level pressure (SLP; Pa), (c) vertical wind shear (VWS; m s^{-1}), (d) 500-hPa vertical p-velocity (10^{-2} Pa s^{-1}), (e) 600-hPa specific humidity (q600; g kg^{-1}), and (f) EKE at 850 hPa (m^2 s^{-2}) in the TC season with respect to the WP_TEJ index. The areas with red (blue) shades indicate areas where the positive (negative) difference is statistically significant at the 95% confidence level based on the F test. The regression is performed with respect to the WP_TEJ index.

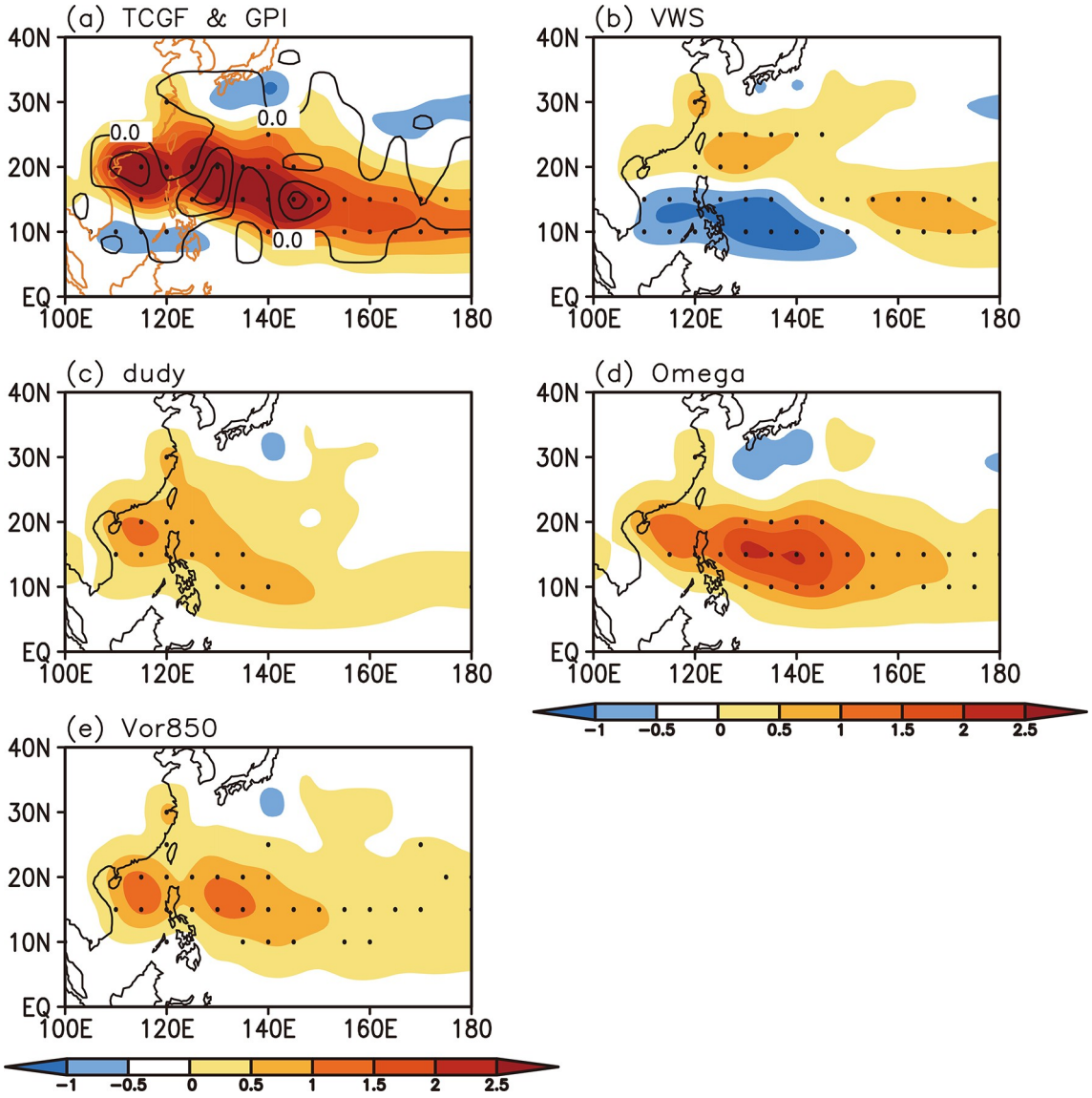

Fig. 7. Composite differences between the strong and weak WP_TEJ years in (a) TCGF density (contour; larger than 0.0 with interval 0.5) and DGPI (shaded) anomalies and (b–e) contributions of the four terms to DGPI anomalies over the WNP. The four terms include (b) vertical wind shear (VWS), (c) meridional gradient of zonal wind (d*u*/d*y*), (d) 500-hPa vertical *p*-velocity (omega), and (e) 850-hPa vorticity (Vor850). The dotted areas indicate areas where the positive (negative) difference is statistically significant at the 95% confidence level based on the Student's *t* test. In (a), TCGF density indicates TCGF binned in each 5° longitude × 5° latitude grid box.

DGPI anomalies correspond well with the positive TCGF anomalies in the strong WP_TEJ years, both prevailing in the main TC genesis region of the WNP. This is consistent with positive correlation between the WP_TEJ index and TCGF over the WNP as shown in Fig. 4. This also indicates that the DGPI indeed has good skill in representing the WNP TCGF variability. We further calculated the relative contribution of each dynamic factor to the DGPI anomalies by varying one variable with the others fixed as in climatology (Figs. 7b–e). Clearly, the positive DGPI anomalies induced by the intensified WP_TEJ were mainly contributed by the anomalous meridional gradient of zonal wind (d*u*/d*y*), midlevel vertical velocity, and 850-hPa vorticity, with the most important factor being the midlevel vertical velocity and the second being the low-level vorticity.

Since the low-level vorticity plays a key role in controlling TC genesis, we estimated the possible contributors leading to the low-level vorticity anomalies based on the relative vorticity tendency equation. Figure 8 shows the regressed patterns in the four terms that contribute to the positive low-level vorticity anomalies averaged over the core region of low-level vorticity anomalies (10°–20°N, 130°–150°E) shown in Fig. 6a. Changes in the low-level relative vorticity are strongly dominated by the divergence term induced by the WP_TEJ. The vertical advection term also contributes to the positive anomalies of the low-level relative vorticity, but the values are much smaller than the divergence term. In contrast, the contributions from the horizontal advec-

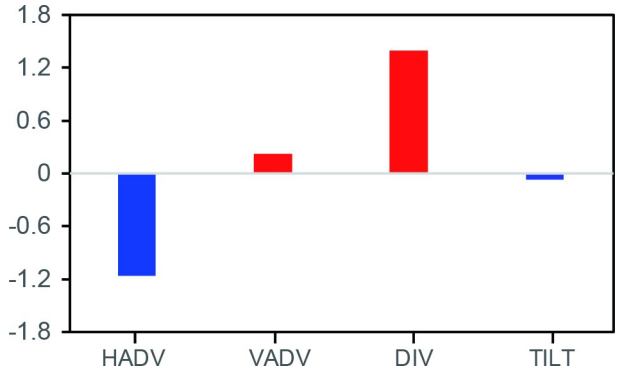

Fig. 8. Regressed contributions to the vorticity budget by horizontal advection term (HADV; 10^{-12} s^{-2}), vertical advection term (VADV; 10^{-12} s^{-2}), divergence term (DIV, 10^{-12} s^{-2}), and tilting term (TILT; 10^{-12} s^{-2}) in the vorticity equation averaged over the region of 10°–20°N, 130°–150°E at 850 hPa.

tion term and the tilting term are negative.

The above results suggest that the midlevel vertical velocity and the low-level vorticity anomalies associated with the intensified WP_TEJ are two key factors to TCGF, while the low-level vorticity anomalies are mainly modulated by the low-level divergence. To understand how the WP_TEJ intensity in the upper troposphere modulates the middle and lower tropospheric thermodynamic and dynamic conditions, we examined the regressed 150-hPa ageostrophic winds, 150-hPa and 850-hPa divergence fields, and vertical circulation averaged between 130°–150°E with respect to the WP_TEJ index, with the results shown in Fig. 9. The intensified upper-level anticyclonic ageostrophic flow (Fig. 9a) with enhanced divergence in the upper troposphere (Fig. 9b) induced by the intensified WP _TEJ is located north of the entrance region of the WP_TEJ, which is consistent with the dynamical forcing of a quasi-geostrophically balanced upper-level jet stream (Uccellini and Johnson, 1979). The upper-level divergence leads to enhanced upward motion throughout the whole troposphere (Fig. 9c) and induces anomalous convergence in the lower troposphere (Fig. 9d). Note that the enhanced upper-level divergence, low-level convergence, and the deep upward motion by the strong WP_TEJ are collocated with the main TC genesis region over the WNP. Therefore, the strong (weak) WP_TEJ can lead to the enhanced (reduced) ageostrophic northerly wind in the upper troposphere in the entrance region of the jet with enhanced (reduced) upper tropospheric divergence, low-level convergence, and deep upward motion to the north of the jet core in the main TC genesis region over the WNP. The low-level convergence (divergence) anomalies further contribute to the positive (negative) low-level relative vorticity and humidity anomalies. As a result, the strong (weak) WP_TEJ exerts favorable (unfavorable) thermodynamic and dynamic conditions for TC genesis over the WNP.

The above results strongly suggest that the WP_TEJ plays an important role in affecting TC genesis over the WNP. However, it is unclear whether the intensity change in the WP_TEJ is the cause or consequence of changes in TC activity because a feedback between the upper-level jet and the TC exists at the synoptic scale (Bosart et al., 2000). That is, diabatic heating in a strong TC can lead to an outflow jet to the southwest of the low-level TC center as the

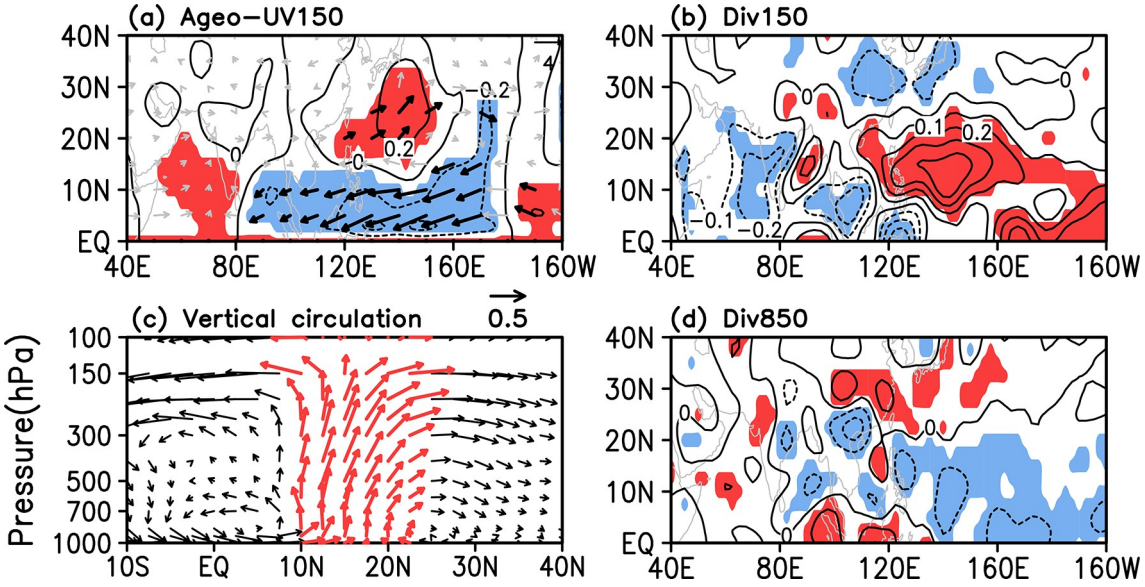

Fig. 9. Regressed patterns of (a) 150-hPa ageostrophic wind (vectors) and meridional velocity (shaded; m s^{-1}), (b) 150-hPa divergence (10^{-6} s^{-1}), (c) vertical circulation averaged between 130°–150°E, and (d) 850-hPa divergence (10^{-6} s^{-1}) in the TC season with respect to the WP_TEJ index. In (a,b,d), the areas with red (blue) shades indicate areas where the positive (negative) difference is statistically significant at the 95% confidence level based on the *F* test. In (c), vertical velocity has been multiplied by 50, and the red arrows indicate areas where the difference is statistically significant at the 95% confidence level by the *F* test.

Rossby wave response (Wang and Holland, 1996), which could affect the location and strength of the upper-level jet. To examine whether the change in the WP_TEJ intensity is the cause or consequence of TC activity, we calculated the lead-lag correlation of daily WP_TEJ index with 500-hPa and 850-hPa vertical *p*-velocity, 850-hPa vorticity and 150-hPa divergence averaged over the region (10°–20°N, 130°–150°E). A maximal positive (negative) correlation with a negative time lag indicates the intensified WP_TEJ leading the TC activity. We can see from Fig. 10 that at the synoptic scale, the strengthened WP_TEJ corresponds to anomalous upper-level divergence (Fig. 10b), upward motion (negative vertical *p*-velocity) in the middle-lower troposphere (Fig. 10a), and the increased low-level vorticity (Fig. 10b), consistent with the seasonal mean fields (Fig. 6). More importantly, the change in the WP_TEJ significantly leads the anomalies in upper-level divergence by two days in terms of the vertical motion at 500 hPa and by two or three days at 850 hPa, and in 850-hPa relative vorticity by about four days. We also tracked each TC genesis and calculated the TCGFs accumulated in different intervals of the pentad-mean WP_TEJ intensity anomalies prior to TC genesis (Fig. 11). In total, about 60% of TCs formed over the WNP when the WP_TEJ intensified within a pentad prior to TC genesis. This strongly demonstrates that the WP_TEJ anomaly is more likely to have driven changes in the thermodynamic and dynamic conditions affecting TC genesis over the WNP, and the feedback of TC activity on the WP_TEJ is secondary.

6. Conclusions and discussion

In this study, the impact of the WP_TEJ on the interannual variability of TCGF over the WNP is examined based on the best-track TC data and global reanalysis. A statistically significant positive correlation on the interannual timescale between the WP_TEJ intensity and the WNP TCGF in the TC season (June–September) is documented, with correlation coefficient of 0.66 during 1980–2020. The associated physical processes are conceptualized in Fig. 12. The

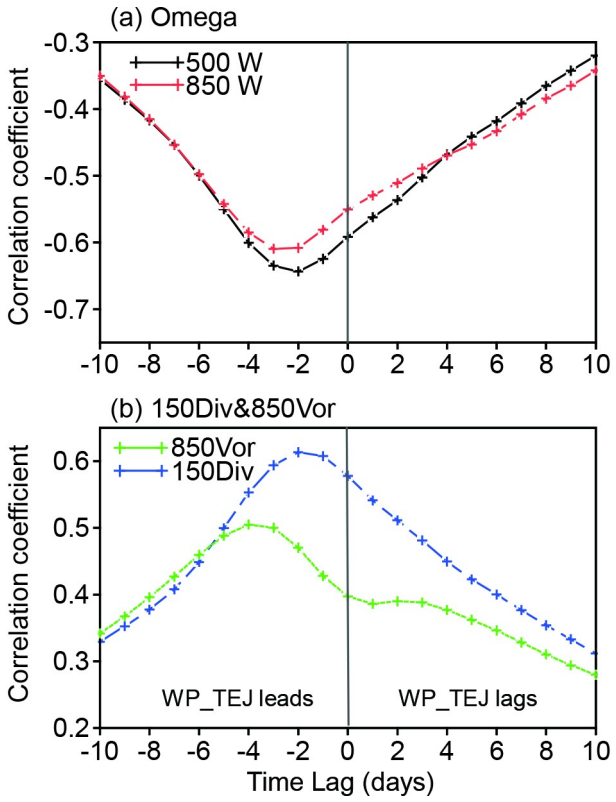

Fig. 10. Lead-lag correlation of the daily WP_TEJ index with 500-hPa and 850-hPa vertical *p*-velocity, 850-hPa vorticity (850Vor), and 150-hPa divergence (150Div) averaged over the region (10°–20°N, 130°–150°E) during 1980–2020. Negative time lags indicate that an intensified WP_TEJ leads the fields examined.

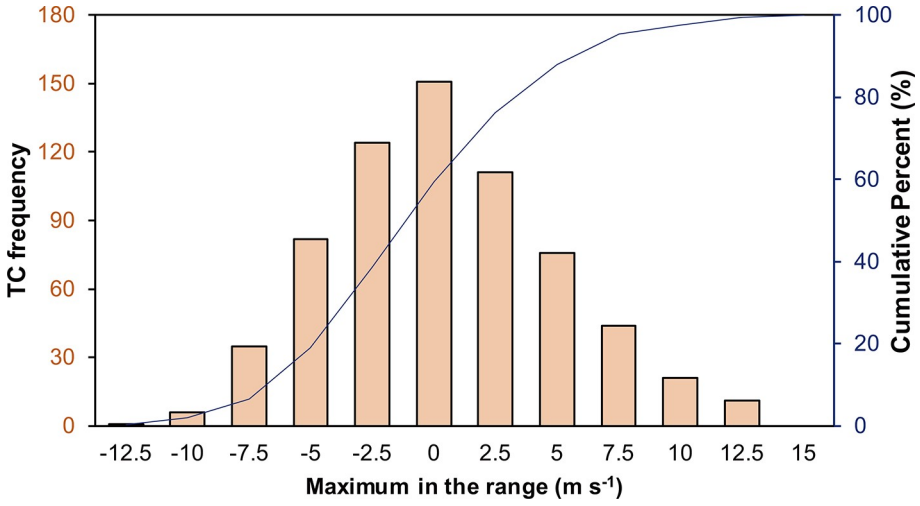

Fig. 11. TC frequency accumulated in the different intervals of the pentad-mean WP_TEJ intensity anomalies prior to TC genesis. The abscissa is aligned with respect to the maximum in the range. For example, a 5-day mean WP_TEJ index in the range larger than or equal to −2.5 and less than 0 will be aligned with 0.

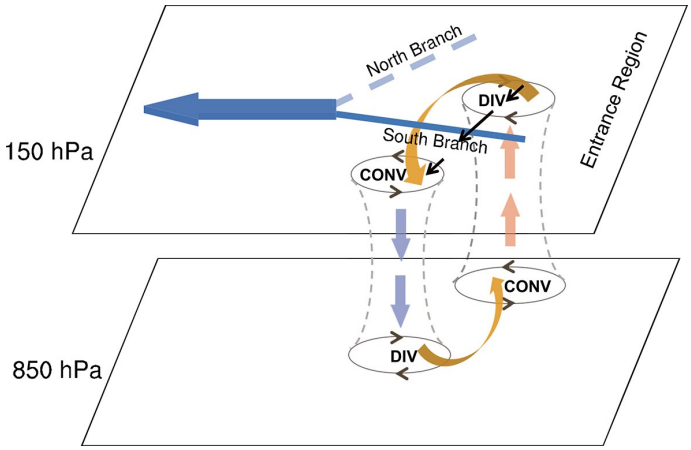

Fig. 12. Schematic diagram showing the processes through which the intensified WP_TEJ affects the WNP environment associated with TC genesis in the TC season.

changes in WP_TEJ intensity affect TC genesis over the WNP by modulating deep upward motion and low-level vorticity. The strengthened WP_TEJ can lead to the enhanced upper-level ageostrophic northerly wind in the entrance region of the jet with enhanced upper tropospheric divergence, deep upward motion, and low-level convergence to the north of the jet core in the main TC genesis region over the WNP. As a result, the strong WP_TEJ exerts a significant influence on the thermodynamic and dynamic conditions affecting TC genesis, including an increase in middle tropospheric humidity, positive anomalies in low-level relative vorticity and EKE, reduced sea level pressure and vertical wind shear over the WNP. These changes are favorable for TC genesis over the WNP. The opposite is true for the weak WP_TEJ.

An interesting issue is what controls the interannual variability of the WP_TEJ intensity. As mentioned in section 1, the TEJ core over the North Indian Ocean is energetically maintained by the meridional thermal contrast between the Tibetan Plateau and the Indian Ocean (Koteswaram, 1958). The interannual variability of the TEJ core is considered to be closely linked to the interannual variability of the Walker and local Hadley circulations induced by the anomalous heating over the Tibetan Plateau, Indian summer monsoon rainfall, and ENSO (Chen and van Loon, 1987; Pattanaik and Satyan, 2000; Rao and Srinivasan, 2016). Although the WP_TEJ is part of the TEJ, the change in the WP_TEJ intensity seems to be independent of that in the TEJ core. Therefore, factors controlling the interannual variability of the WP_TEJ intensity might be different from that of the TEJ core, although the basic principles, such as the thermal wind balance, resulting in the upper-level jet changes, are similar to each other. We examined the composite differences between the strong and weak WP_TEJ years in tropospheric air temperature averaged between 500 and 150 hPa, precipitation, and SST (Fig. 13). As expected, the intensified WP_TEJ is accompanied by the increased meridional thermal contrast between the tropical western Pacific and

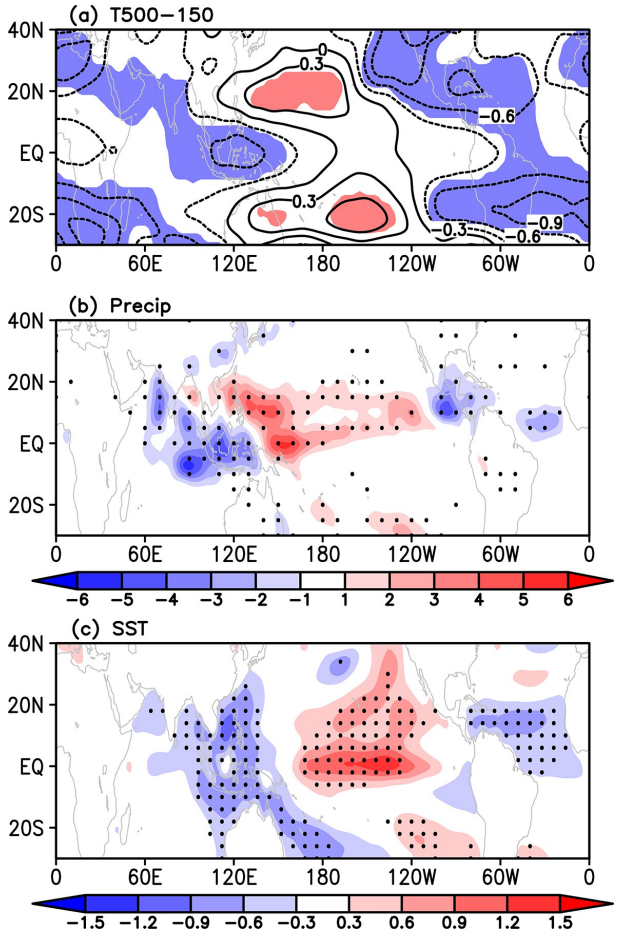

Fig. 13. The composite differences between the strong and weak years in (a) tropospheric air temperature (K) averaged within the layer between 500–150 hPa, (b) precipitation (mm d^{-1}) and (c) SST (K). In (a), the contour indicates the difference, and the areas with red (blue) shading indicate areas where the positive (negative) difference is statistically significant at the 95% confidence level based on the Student's *t* test. In (b) and (c), the shading indicates the differences, and the dotted areas indicate areas where the positive (negative) difference is statistically significant at the 95% confidence level based on the Student's *t* test.

the Maritime Continent (Fig. 13a), which can be explained by the thermal wind balance. When the WP_TEJ intensified, there is more precipitation over the tropical western Pacific and less precipitation over the Maritime Continent and the North Indian Ocean. The composite difference in SST shows a pattern like ENSO Modoki. The former might be related to the anomalous local Hadley circulation, while the latter contributes to the changes in the Walker circulation. Therefore, it is not unreasonable to hypothesize that the interannual variability of the WP_TEJ intensity might be related to the interannual variability of the Walker and local Hadley circulations induced by the western Pacific summer monsoon rainfall and ENSO Modoki, respectively. However, the detailed mechanisms and their relative importance need further examination in future work.

Acknowledgements. This study is supported by the Guangdong Major Project of Basic and Applied Basic Research (Grant No. 2020B0301030004), the National Natural Science Foundation of China (Grant Nos. 42075015, 41775060, and 41875114), and the Science and Technology Commission of Shanghai Municipality, China (Grant No. 20dz1200700). The CMA best track TC dataset was downloaded from http://tcdata.typhoon.org.cn/. The JTWC best track TC dataset was from http://www.jma.go.jp/jma/jma-eng/jma-center/rsmc-hp-pub-eg/besttrack.html. The JMA best track TC dataset was downloaded from http://www.jma.go.jp/jma/jma-eng/jma-center/rsmc-hp-pub-eg/besttrack.html. The NCEP–NCAR reanalysis data were downloaded from https://www.esrl.noaa.gov/psd/data/gridded/data.ncep.reanalysis.html. The ERSST v5 analyses were downloaded from https://www.esrl.noaa.gov/psd/data/gridded/data.noaa.ersst.v5.html. The CMAP data were downloaded from https://www.esrl.noaa.gov/psd/data/gridded/data.cmap.html.

REFERENCES

Besson, L., and Y. Lemaître, 2014: Mesoscale convective systems in relation to African and tropical easterly jets. *Mon. Wea. Rev.*, **142**, 3224–3242, https://doi.org/10.1175/MWR-D-13-00247.1.

Bosart, L. F., W. E. Bracken, J. Molinari, C. S. Velden, and P. G. Black, 2000: Environmental influences on the rapid intensification of Hurricane Opal (1995) over the Gulf of Mexico. *Mon. Wea. Rev.*, **128**, 322–352, https://doi.org/10.1175/1520-0493(2000)128<0322:EIOTRI>2.0.CO;2.

Chan, J. C. L., 2005: Interannual and interdecadal variations of tropical cyclone activity over the western North Pacific. *Meteorol. Atmos. Phys.*, **89**, 143–152, https://doi.org/10.1007/s00703-005-0126-y.

Chen, G. H., and C.-Y. Tam, 2010: Different impacts of two kinds of Pacific Ocean warming on tropical cyclone frequency over the western North Pacific. *Geophys. Res. Lett.*, **37**, L01803, https://doi.org/10.1029/2009GL041708.

Chen, H., 2006: A climatological study on the tropical easterly jet and Asian summer monsoon. *M.S. thesis*, 18pp, https://doi.org/10.7666/d.y868392. (in Chinese with English abstract)

Chen, H., Y.-H. Ding, and J.-H. He, 2007: The structure and variation of tropical easterly jet and its relationship with the monsoon rainfall in Asia and Africa. *Chinese Journal of Atmospheric Sciences*, **31**, 926–936, https://doi.org/10.3878/j.issn.1006-9895.2007.05.16. (in Chinese with English abstract)

Chen, T.-C., and H. van Loon, 1987: Interannual variation of the tropical easterly jet. *Mon. Wea. Rev.*, **115**, 1739–1759, https://doi.org/10.1175/1520-0493(1987)115<1739:IVOTTE>2.0.CO;2.

Chia, H. H., and C. F. Ropelewski, 2002: The interannual variability in the genesis location of tropical cyclones in the Northwest Pacific. *J. Climate*, **15**, 2934–2944, https://doi.org/10.1175/1520-0442(2002)015<2934:TIVITG>2.0.CO;2.

Emanuel, K., 2018: 100 years of progress in tropical cyclone research. *Meteor. Monographs*, **59**, 15.1–15.68, https://doi.org/10.1175/AMSMONOGRAPHS-D-18-0016.1.

Fischer, M. S., B. H. Tang, and K. L. Corbosiero, 2017: Assessing the influence of upper-tropospheric troughs on tropical cyclone intensification rates after genesis. *Mon. Wea. Rev.*, **145**, 1295–1313, https://doi.org/10.1175/MWR-D-16-0275.1.

Fischer, M. S., B. H. Tang, and K. L. Corbosiero, 2019: A climatological analysis of tropical cyclone rapid intensification in environments of upper-tropospheric troughs. *Mon. Wea. Rev.*, **147**, 3693–3719, https://doi.org/10.1175/MWR-D-19-0013.1.

Fontaine, B., and S. Janicot, 1992: Wind-field coherence and its variations over West Africa. *J. Climate*, **5**, 512–524, https://doi.org/10.1175/1520-0442(1992)005<0512:WFCAIV>2.0.CO;2.

Gray, W. M., 1968: Global view of the origin of tropical disturbances and storms. *Mon. Wea. Rev.*, **96**, 669–700, https://doi.org/10.1175/1520-0493(1968)096<0669:GVOTOO>2.0.CO;2.

Guo, Y.-P., and Z.-M. Tan, 2018: Impacts of the boreal spring Indo-Pacific warm pool Hadley circulation on tropical cyclone activity over the western North Pacific. *J. Climate*, **31**, 1361–1375, https://doi.org/10.1175/JCLI-D-17-0422.1.

Holton, J. R., and D. O. Staley, 1973: An introduction to dynamic meteorology. *American Journal of Physics*, **41**, 752–754, https://doi.org/10.1119/1.1987371.

Huang, S. H., B. Wang, and Z. P. Wen, 2020: Dramatic weakening of the tropical easterly jet projected by CMIP6 Models. *J. Climate*, **33**, 8439–8455, https://doi.org/10.1175/JCLI-D-19-1002.1.

Kalnay, E., and Coauthors, 1996: The NCEP/NCAR 40-year reanalysis project. *Bull. Amer. Meteor. Soc.*, **77**, 437–472, https://doi.org/10.1175/1520-0477(1996)077<0437:TNYRP>2.0.CO;2.

Klotzbach, P., and Coauthors, 2019: Seasonal tropical cyclone forecasting. *Tropical Cyclone Research and Review*, **8**, 134–149, https://doi.org/10.1016/j.tcrr.2019.10.003.

Koteswaram, P., 1958: The easterly jet stream in the tropics. *Tellus*, **10**, 43–57, https://doi.org/10.3402/tellusa.v10i1.9220.

Krishnamurti, T. N., and H. N. Bhalme, 1976: Oscillations of a monsoon system. *Part I. Observational aspects. J. Atmos. Sci.*, **33**, 1937–1954, https://doi.org/10.1175/1520-0469(1976)033<1937:OOAMSP>2.0.CO;2.

Krishnamurti, T. N., N. Karmakar, V. Misra, B. Nag, D. Sahu, S. Dubey, and Z. Haddad, 2018: Association between upper level diffluence in the tropical easterly jet and the formation of the strongest Atlantic hurricanes in recent years. *Proc. SPIE 10782, Remote Sensing and Modeling of the Atmosphere, Oceans, and Interactions VII*, Honolulu, SPIE, 1078206pp, https://doi.org/10.1117/12.2500287.

Lemburg, A., J. Bader, and M. Claussen, 2019: Sahel rainfall-tropical easterly jet relationship on synoptic to intraseasonal

time scales. *Mon. Wea. Rev.*, **147**, 1733–1752, https://doi.org/10.1175/MWR-D-18-0254.1.

Li, Y., Y. H. Ding, and W. J. Li, 2017: Interdecadal variability of the Afro-Asian summer monsoon system. *Adv. Atmos. Sci.*, **34**, 833–846, https://doi.org/10.1007/s00376-017-6247-7.

Liang, B. Q., 1990: *Tropical Meteorology*. Sun Yat-sen University Press, 101–104. (in Chinese)

Lu, J. X., and Y. H. Ding, 1989: Climatic study on the summer tropical easterly jet at 200hPa. *Adv. Atmos. Sci.*, **6**, 215–226, https://doi.org/10.1007/BF02658017.

Nicholson, S. E., 2009: On the factors modulating the intensity of the tropical rainbelt over West Africa. *International Journal of Climatology*, **29**, 673–689, https://doi.org/10.1002/joc.1702.

Pattanaik, D. R., and V. Satyan, 2000: Fluctuations of tropical easterly jet during contrasting monsoons over India: A GCM study. *Meteor. Atmos. Phys.*, **75**, 51–60, https://doi.org/10.1007/s007030070015.

Pfeffer, R. L., and M. Challa, 1981: A numerical study of the role of eddy fluxes of momentum in the development of Atlantic hurricanes. *J. Atmos. Sci.*, **38**, 2393–2398, https://doi.org/10.1175/1520-0469(1981)038<2393:ANSOTR>2.0.CO;2.

Rao, S., and J. Srinivasan, 2016: The impact of latent heating on the location and strength of the tropical easterly jet. *Meteorol. Atmos. Phys.*, **128**, 247–261, https://doi.org/10.1007/s00703-015-0407-z.

Rao, V. B., C. C. Ferreira, S. H. Franchito, and S. S. V. S. Ramakrishna, 2008: In a changing climate weakening tropical easterly jet induces more violent tropical storms over the north Indian Ocean. *Geophys. Res. Lett.*, **35**, L15710, https://doi.org/10.1029/2008GL034729.

Sears, J., and C. S. Velden, 2014: Investigating the role of the upper-levels in tropical cyclone genesis. *Tropical Cyclone Research and Review*, **3**, 91–110, https://doi.org/10.6057/2014TCRR02.03.

Smith, T. M., and R. W. Reynolds, 2004: Improved extended reconstruction of SST (1854–1997). *J. Climate*, **17**, 2466–2477, https://doi.org/10.1175/1520-0442(2004)017<2466:IEROS>2.0.CO;2.

Uccellini, L. W., and D. R. Johnson, 1979: The coupling of upper and lower tropospheric jet streaks and implications for the development of severe convective storms. *Mon. Wea. Rev.*, **107**, 682–703, https://doi.org/10.1175/1520-0493(1979)107<0682:TCOUAL>2.0.CO;2.

Vashisht, A., B. Zaitchik, and A. Gnanadesikan, 2021: ENSO teleconnection to eastern African summer rainfall in global climate models: Role of the tropical easterly jet. *J. Climate*, **34**, 293–312, https://doi.org/10.1175/JCLI-D-20-0222.1.

Wang, B., and J. C. L. Chan, 2002: How strong ENSO events affect tropical storm activity over the western North Pacific. *J. Climate*, **15**, 1643–1658, https://doi.org/10.1175/1520-0442(2002)015<1643:HSEEAT>2.0.CO;2.

Wang, B., and H. Murakami, 2020: Dynamic genesis potential index for diagnosing present-day and future global tropical cyclone genesis. *Environmental Research Letters*, **15**, 114008, https://doi.org/10.1088/1748-9326/abbb01.

Wang, C., and L. G. Wu, 2016: Interannual shift of the tropical upper-tropospheric trough and its influence on tropical cyclone formation over the western North Pacific. *J. Climate*, **29**, 4203–4211, https://doi.org/10.1175/JCLI-D-15-0653.1.

Wang, C., and B. Wang, 2021: Impacts of the South Asian high on tropical cyclone genesis in the South China Sea. *Climate Dyn.*, **56**, 2279–2288, https://doi.org/10.1007/s00382-020-05586-8.

Wang, C., K. Wu, L. G. Wu, H. K. Zhao, and J. Cao, 2021: What caused the unprecedented absence of western North Pacific tropical cyclones in July 2020. *Geophys. Res. Lett.*, **48**, e2020GL092282, https://doi.org/10.1029/2020GL092282.

Wang, H. J., J. Q. Sun, and K. Fan, 2007: Relationships between the North Pacific oscillation and the typhoon/hurricane frequencies. *Science in China Series D: Earth Sciences*, **50**, 1409–1416, https://doi.org/10.1007/s11430-007-0097-6.

Wang, Y. Q., and G. J. Holland, 1996: The beta drift of baroclinic vortices. *Part II: Diabatic vortices. J. Atmos. Sci.*, **53**, 3737–3756, https://doi.org/10.1175/1520-0469(1996)053<3737:TBDOBV>2.0.CO;2.

Wu, L., H. J. Zhang, J.-M. Chen, and T. Feng, 2018: Impact of two types of El Niño on tropical cyclones over the western North Pacific: Sensitivity to location and intensity of Pacific warming. *J. Climate*, **31**, 1725–1742, https://doi.org/10.1175/JCLI-D-17-0298.1.

Xie, P. P., and P. A. Arkin, 1997: Global precipitation: A 17-year monthly analysis based on gauge observations, satellite estimates, and numerical model outputs. *Bull. Amer. Meteor. Soc.*, **78**, 2539–2558, https://doi.org/10.1175/1520-0477(1997)078<2539:GPAYMA>2.0.CO;2.

Yang, Y. Z., 1980: Primary analysis of the formation and development of the tropical easterly over the upper troposphere. *Proceedings of the Tropical Weather Conference*, Science Press. (in Chinese)

Yu, J. H., T. Li, Z. M. Tan, and Z. W. Zhu, 2016: Effects of tropical North Atlantic SST on tropical cyclone genesis in the western North Pacific. *Climate Dyn.*, **46**, 865–877, https://doi.org/10.1007/s00382-015-2618-x.

Zhan, R. F., Y. Q. Wang, and X. T. Lei, 2011: Contributions of ENSO and East Indian Ocean SSTA to the interannual variability of Northwest Pacific tropical cyclone frequency. *J. Climate*, **24**, 509–521, https://doi.org/10.1175/2010JCLI3808.1.

Zhan, R. F., Y. Q. Wang, and M. Ying, 2012: Seasonal forecasts of tropical cyclone activity over the western North Pacific: A review. *Tropical Cyclone Research and Review*, **1**, 307–324, https://doi.org/10.6057/2012TCRR03.07.

Zhan, R. F., Y. Q. Wang, and M. Wen, 2013: The SST gradient between the southwestern Pacific and the western Pacific warm pool: A new factor controlling the northwestern Pacific tropical cyclone genesis frequency. *J. Climate*, **26**, 2408–2415, https://doi.org/10.1175/JCLI-D-12-00798.1.

Zhan, R. F., Y. Q. Wang, and J. W. Zhao, 2019: Contributions of SST anomalies in the Indo-Pacific Ocean to the interannual variability of tropical cyclone genesis frequency over the western North Pacific. *J. Climate*, **32**, 3357–3372, https://doi.org/10.1175/JCLI-D-18-0439.1.

Zhang, L. L., 1986: The upper-level southern easterly jet and the activity of typhoon. *Journal of Tropical Meteorology*, **2**, 62–70. (in Chinese with English abstract)

Zhang, W., G. A. Vecchi, H. Murakami, G. Villarini, and L. Jia, 2016: The Pacific Meridional Mode and the occurrence of tropical cyclones in the western North Pacific. *J. Climate*, **29**, 381–398, https://doi.org/10.1175/JCLI-D-15-0282.1.

Zhou, B. T., and X. Cui, 2008: Hadley circulation signal in the tropical cyclone frequency over the western North Pacific. *J. Geophys. Res.*, **113**, D16107, https://doi.org/10.1029/2007JD009156.